

Energy-scale phenomenology and pairing via resonant spin-charge motion in FeAs, CuO, heavy-fermion and other exotic superconductors

Y. J. Uemura

Department of Physics, Columbia University, 538 West 120th Street, New York, NY 10027, USA

Abstract

Muon spin relaxation (μ SR) studies of the “1111” and “122” FeAs systems have detected static magnetism with variably sized ordered moments in their parent compounds. The phase diagrams of FeAs, CuO, organic BEDT, A_3C_{60} and heavy-fermion systems indicate competition between static magnetism and superconductivity, associated with first-order phase transitions at quantum phase boundaries. In both FeAs and CuO systems, the superfluid density n_s/m^* at $T \rightarrow 0$ exhibits a nearly linear scaling with T_c . Analogous to the roton-minimum energy scaling with the lambda transition temperature in superfluid ^4He , clear scaling with T_c was also found for the energy of the magnetic resonance mode in cuprates, $(\text{Ba,K})\text{Fe}_2\text{As}_2$, CeCoIn_5 and CeCu_2Si_2 , as well as the energy of the superconducting coherence peak observed by angle resolved photo emission (ARPES) in the cuprates near $(\pi,0)$. Both the superfluid density and the energy of these pair-non-breaking soft-mode excitations determine the superconducting T_c via phase fluctuations of condensed bosons. Combining these observations and common dispersion relations of spin and charge collective excitations in the cuprates, we propose a resonant spin charge motion/coupling, “traffic-light resonance,” expected when the charge energy scale ϵ_F becomes comparable to the spin fluctuation energy scale $\hbar\omega_{SF} \sim J$, as the process which leads to pair formation in these correlated electron superconductors.

Key words: FeAs systems, high- T_c cuprates, magnetic resonance mode, spin-mediated pairing
PACS: 74.70.Tx, 74.62.Fj, 74.25.Fy, 74.25.Dw

1. Introduction

Discovery of superconductivity in the $\text{La}(\text{O,F})\text{FeAs}$ system [1] and the subsequent development of the superconducting $\text{RE}(\text{O,F})\text{FeAs}$ (RE= rare earth La, Nd, Ce, Sm, ...; “1111”) [2] and $(\text{A,K})\text{Fe}_2\text{As}_2$ (A = Ba, Sr, Ca; “122”) systems [3,4,5] have generated renewed excitement and interest in studies of superconductivity in correlated electron systems. In this paper, we first review recent muon spin relaxation (μ SR) measurements of static magnetic order and superfluid density in the 1111 and 122 FeAs systems, and compare the results with those for high- T_c cuprates, organic BEDT, A_3C_{60} and other exotic superconductors. We then look into energy scales of the magnetic resonance mode (observed by inelastic neutron scattering) and of the superconducting coherence peak (by ARPES), and suggest that both of these are manifestations of soft-mode excitations analogous to rotons in superfluid ^4He . After discussing

the roles of the superfluid density and the soft-mode energy scales in determining T_c , we will propose a pairing mechanism in correlated-electron superconductors based on a resonant spin-charge motion/coupling, which we term as “traffic-light resonance.” The original ideas of this picture were presented in refs. [6,7].

2. Magnetic order of the FeAs systems

Static magnetic order in the undoped and lightly-doped compounds of the 1111 and 122 FeAs families has been studied by neutron scattering [8,9,10], μ SR [11,12,13,14,15,16] and Moessbauer-effect measurements [11,17,18]. All the undoped systems exhibit long-range collinear antiferromagnetic (AF) order of Fe moments [8,9,10]. The size of the ordered moment can be estimated from the hyperfine field in Moessbauer experiments and μ SR precession frequencies ν in zero field. Since the hyperfine coupling constants between Fe moments and muon spins are nearly equal (difference $< 10\%$) for the 1111 and 122 compounds [15], the μ SR frequency ν represents

* Corresponding author. Tel/Fax: +1 212 854 8370
Email address: tomo@lorentz.phys.columbia.edu (Y. J. Uemura).

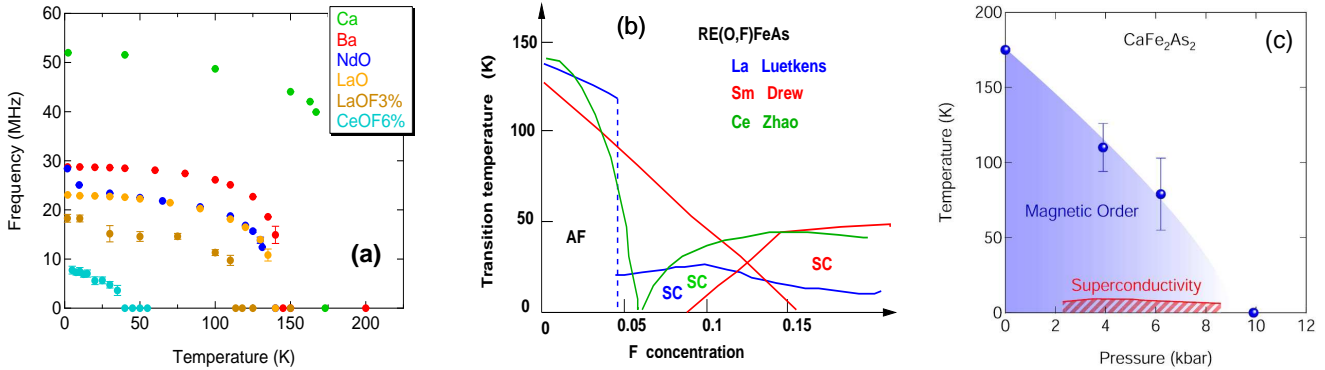


Fig. 1. (a) Temperature dependence of the muon spin precession frequency ν observed in zero field in CaFe₂As₂ [16], BaFe₂As₂, NdOFeAs [15], LaOFeAs, La(O_{0.97}F_{0.03})FeAs [14], and Ca(O_{0.94}F_{0.06})FeAs [19]. (b) Phase diagrams of RE(O,F)FeAs systems obtained for RE = La by Luetkens *et al.* [20] (blue lines), RE = Sm by Drew *et al.* [21] (red) based on μ SR measurements, and RE = Ce by Zhao *et al.* [22] (green) on neutron measurements in ambient pressure. (c) Phase diagram of CaFe₂As₂ in applied pressure based on μ SR results by Goko *et al.* [16] for magnetic order and transport results [4] for superconductivity.

the temperature and system variation of the ordered Fe moment.

Figure 1(a) shows our μ SR results on several non-superconducting undoped and lightly-doped 1111 [14,15] and 122 compounds [15,16,19]. This figure demonstrates that the size of the ordered Fe moments varies continuously from ~ 0.1 to 1.0 Bohr magnetons, nearly scaling with T_N . This feature contrasts clearly with cuprate systems with static AF or stripe spin order, which almost always appears with ordered moment size ~ 0.5 Bohr magnetons per Cu at $T \rightarrow 0$. The variable moment size in FeAs systems suggests an itinerant character of 3-d electrons forming multiple bands.

Figure 1(b) shows the magnetic and superconducting phase diagrams of the 1111 FeAs systems reported for RE=La by Luetkens *et al.* [20] (blue lines) and RE=Sm by Drew *et al.* [21] (red) both based on μ SR, and for RE=Ce by Zhao *et al.* [22] (green) on neutron measurements. The evolution from AF to superconducting (SC) states occurs with abrupt first-order-like change in the La systems, second-order-like change in the Ce systems, and associated with a region of coexisting magnetism and superconductivity in the Sm systems. In ZF- μ SR studies on CeO_{0.94}F_{0.06}FeAs [19] using the same sample studied by Zhao *et al.* [22], we found a short-range static magnetic order developing below $T = 40$ K as shown in Fig. 1(a). This makes the RE=Ce phase diagram closer to those of RE=La and Sm.

Superconductivity in the 122 (A,K)Fe₂As₂ (A = Ca,Ba,Sr) systems can be obtained by hole doping [3] as well as by application of hydrostatic pressure to the undoped parent compounds [4,5]. In both cases, our μ SR studies [15,16] have revealed that superconducting specimens exhibit static magnetic order in a partial volume fraction, typically ~ 50 % of the total volume. Figure 1(c) shows the phase diagram for CaFe₂As₂ in hydrostatic pressure, based on our μ SR results for static magnetic order [16] and resistivity / susceptibility results [4,23] for superconductivity. Magnetic order survives in a partial volume

fraction over the superconducting dome, indicating that magnetism is stronger in the 122 systems than in the 1111 family, probably due to the more 3-dimensional nature of the 122 systems.

At this moment, there is no information on the length scale of the segregation. It is also unclear whether superconductivity occurs exclusively in volumes without static magnetic order or if it prevails over the entire volume. Evolution from the AF to SC state is also associated with phase separation in the cuprates near the static stripe order, where μ SR studies found microscopic segregation with a length scale comparable to the in-plane coherence length and superconductivity surviving exclusively in volumes without static magnetism [24,25,26]. We consider that this is a likely scenario for the 122 FeAs systems as well.

With increasing pressure and decreasing unit-cell volume, superconductivity in organic (BEDT-TTF)₂-X [27] and alkali-doped A₃C₆₀ [28] appears adjacent to static magnetic order. Phase diagrams of BEDT, A₃C₆₀, cuprates, heavy-fermion, and FeAs systems suggest that superconductivity and antiferromagnetism compete for the ground state. The evolution is often associated with a first-order transition, as spatial phase separation was found in the cuprates [24,25,26], CeCu₂Si₂ [29], BEDT [27] and 122 FeAs [15,16] while abrupt change was found in CeRhIn₅ [30], A₃C₆₀ [28] and RE=La 1111 FeAs [20]. Note that superfluid ⁴He exhibits similar first-order quantum transition from the hcp solid to superfluid state with decreasing pressure. The relevance of this phenomenon shall be discussed in the following sections.

Phase separation between volumes with and without static magnetic order has also been detected by μ SR in the insulating frustrated square lattice J₁-J₂ system Cu(Cl,Br)La(Nb,Ta)₂O₇ at the boundary between collinear AF and spin-gapped states [31]. This similarity suggests an important role played by spin frustration in determining the magnetic states of the FeAs systems [32,33]. The itinerant electron aspect and the J₁-J₂ frustration should be viewed not necessarily as contradictory

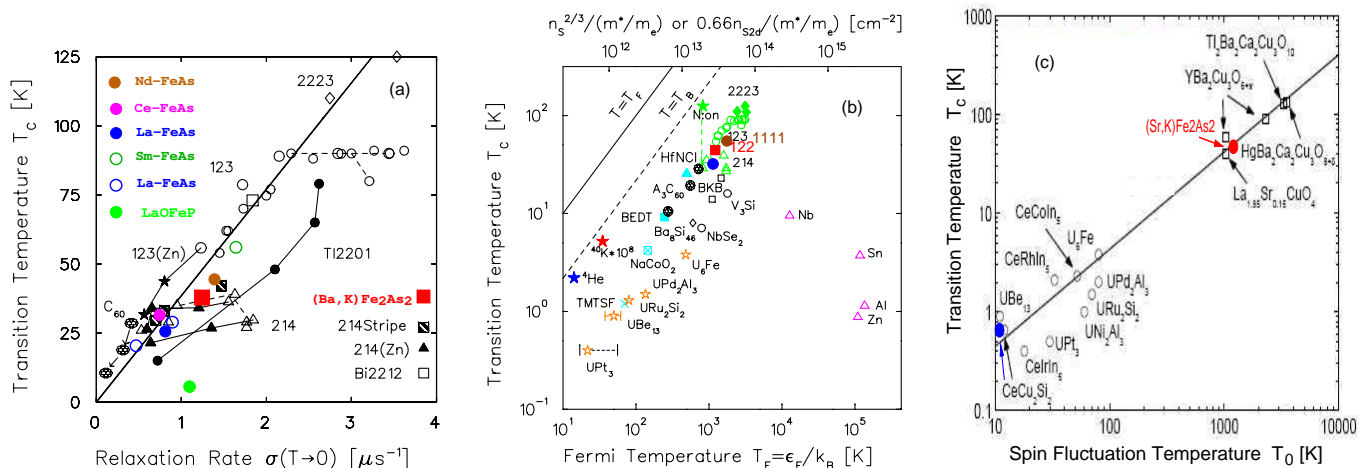


Fig. 2. (a) Plot of T_c versus the muon spin relaxation rate $\sigma(T \rightarrow 0)$ observed by TF- μ SR measurements on cuprates [34,37,38,39,7], 1111 FeAs [12,14] (Ba,K)Fe₂As₂ [16], LaOFeP [14], A₃C₆₀ [38], and various other exotic superconductors [39,7]. The relaxation rate σ is related to the London penetration depth λ , superconducting carrier density n_s , and effective mass m^* as $\sigma \propto 1/\lambda^2 \propto n_s/m^*$. (b) Plot of T_c versus the effective Fermi temperature T_F derived from the μ SR results on superfluid density n_s/m^* for 2-dimensional, and from n_s/m^* combined with the Sommerfeld constant or Pauli susceptibility for 3-d systems [37,38,7]. T_B denotes the Bose-Einstein condensation temperature for a non-interacting Bose gas of corresponding boson density $n_b = n_s/2$ and mass $m_b = 2m^*$. (c) Plot of T_c versus spin fluctuation energy scale T_0 , estimated theoretically based on normal-state transport, susceptibility and specific-heat results for cuprates and heavy fermion systems made by Moriya and Ueda [40]. Also included are points for CeCu₂Si₂ (blue solid circle) based on inelastic neutron scattering results [41,42] and for (Sr,K)Fe₂As₂ (red solid circle) based on neutron scattering results of spin waves in SrFe₂As₂ [43].

concepts, but rather as interplaying elements of the physics in FeAs superconductors.

3. Superfluid energy scales

In type-II superconductors, the London penetration depth λ can be determined from the muon spin relaxation rate σ defined for the Gaussian relaxation envelope $\exp(-\sigma^2 t^2/2)$ observed in a high transverse external field (TF), as

$$\sigma \propto 1/\lambda^2 \propto n_s/m^* \quad (1),$$

where n_s is the superconducting carrier density, m^* is the effective mass, and the clean limit is assumed here for simplicity [34,35,36]. TF- μ SR measurements have been performed on several 1111 and 122 FeAs superconductors [12,14,15,13]. Figure 2(a) shows a plot of $\sigma(T \rightarrow 0)$ versus T_c . The results from FeAs systems follow the nearly linear trend found for cuprates, A₃C₆₀ and organic BEDT systems [34,37,38,39,7]. In theories based on BCS condensation, the transition temperature T_c is related to the energy scale of attractive interaction represented by the gap energy, while one expects only weak and indirect dependence of T_c on n_s . In contrast, if T_c is governed by the acquisition of phase coherence as in Bose-Einstein (BE) condensation of pre-formed pairs, one expects a direct correlation between T_c and n_s . The remarkable universality in Fig. 2(a) suggests strong relevance of the latter case to condensation in all these exotic superconductors, including FeAs systems.

This point can be further appreciated if we convert the horizontal axis to “effective Fermi energy” ϵ_F [37], which is proportional to n_s/m^* in 2-dimensional (2-d) systems. For

3-d systems, ϵ_F can be derived by combining n_s/m^* with another parameter, such as the Sommerfeld constant. The resulting plot of T_c versus ϵ_F is shown in Fig. 2(b), where the BE condensation temperature T_{BE} of an ideal non-interacting Bose gas is shown by the broken line. Although their actual T_c ’s are lower than T_{BE} by about a factor of 4-5, cuprates, FeAs, A₃C₆₀, organic BEDT, and some heavy-fermion systems exhibit the highest ratios T_c/ϵ_F of T_c with respect to the kinetic energy ϵ_F of superconducting carriers.

In Fig. 2(a), we also include a point for LaOFeP [14], which does not follow the linear trend. It has been known for many years that the 214 cuprate systems “branch off” from the linear trend [34], leading the optimally doped 214 LSCO superconductor to have T_c about a factor 2 lower than the 123 YBCO system with the same superfluid density. These features suggest that n_s/m^* is not the sole factor for determination of T_c . Closeness to the competing state with static magnetic order is likely the reason why LSCO and LaOFeP systems have relatively low T_c ’s with respect to their superfluid densities. In Fig. 2(b), we include a point corresponding to superfluid ⁴He. The superfluid transition of ⁴He occurs at $T = 2.2$ K in ambient pressure, which is reduced by about 30 % from $T_{BE} = 3.2$ K for a non-interacting Bose gas with corresponding boson density and mass. Understanding the mechanisms for “reduction” of T_c in these cases would help identifying the additional factor(s) which determine T_c in correlated electron systems.

Before discussing about competing states, let us also look into a spin energy scale. Moriya and Ueda [40] derived a “spin fluctuation temperature” T_0 from transport, susceptibility and specific-heat measurements as the energy scale expected for spin fluctuations at the zone boundary. As

shown in Fig. 2(c), they found a nearly linear correlation between T_c and T_0 . Although T_0 was derived through a theoretical model, this parameter is close to the actual energy scale observed in inelastic neutron scattering, as demonstrated by the point for CeCu_2Si_2 (blue solid circle) representing available neutron results [41,42]. In this figure, we also include a point for $(\text{Sr,K})\text{Fe}_2\text{As}_2$ (red solid circle) based on its T_c and spin wave dispersions measured in SrFe_2As_2 [43]. Comparison of Figs. 2(b) and 2(c) reveals a remarkable correspondence of charge (T_F) and spin (T_0) energy scales in many exotic superconductors. This feature shall be discussed in sections 6 and 7.

4. Magnetic resonance mode and He rotons: soft-mode excitations towards competing states

In the case of superfluid ^4He , collective excitations of rotons provide a channel for thermal depletion of condensed bosons. Thanks to the large phase-space factor for substantial momentum transfer, the roton-minimum energy $\hbar\omega_{\text{roton}}$ plays a dominant role in determining superfluid T_c , as was noticed by Landau and Ruvelds [44]. The experimental confirmation of this concept can be obtained by plotting early neutron results [45] of $\hbar\omega_{\text{roton}}$ versus the superfluid lambda temperature T_c in ambient and applied pressure. The nearly linear relationship shown in Fig. 3 verifies that the roton energy determines T_c of the superfluid state. Rotons are soft-mode phonons related to solid hcp He, whose energy reflects the “closeness” of the superfluid state to the adjacent and competing solid He state. Here we find a good example of how the competing state influences superconducting or superfluid transitions, by providing thermodynamically excitable soft collective modes. This process does not involve “pair-breaking,” but rather puts a condensed boson into a state with different phase. Soft-mode excitation is thus a process of phase fluctuation, distinct from the Kosterlitz-Thouless process due to low dimensionality [46].

The magnetic resonance mode (MRM), observed by inelastic neutron scattering, is a likely candidate for an analogous soft mode in correlated-electron superconductors. Figure 3 demonstrates that the mode energy $\hbar\omega_{\text{MR}}$ of the MRM of various cuprates [47] scales with their T_c , and the ratios $T_c/\hbar\omega_{\text{MR}}$ (slope in Fig. 3) are comparable to that of rotons. The MRM is a spin soft mode related to the stripe spin-charge ordered state in the cuprates. Recent neutron studies revealed an “hour-glass-shape” dispersion relation of this mode [48,49]. For consideration of thermodynamic effects, one should use the low energy peak of populated states on the hour-glass dispersion, which is often denoted as the “spin gap energy.” The spin gap energy, shown by solid square symbols in Fig. 3, exhibits even better agreement with the slope $T_c/\hbar\omega_{\text{roton}}$ of rotons in ^4He .

Very recently, the MRM was also observed in $(\text{Ba,K})\text{Fe}_2\text{As}_2$ [50], CeCoIn_5 [51], and CeCu_2Si_2 [52]. Amazingly, the points for these systems closely follow the roton relationship in Fig. 3. In general, the excitation energy of

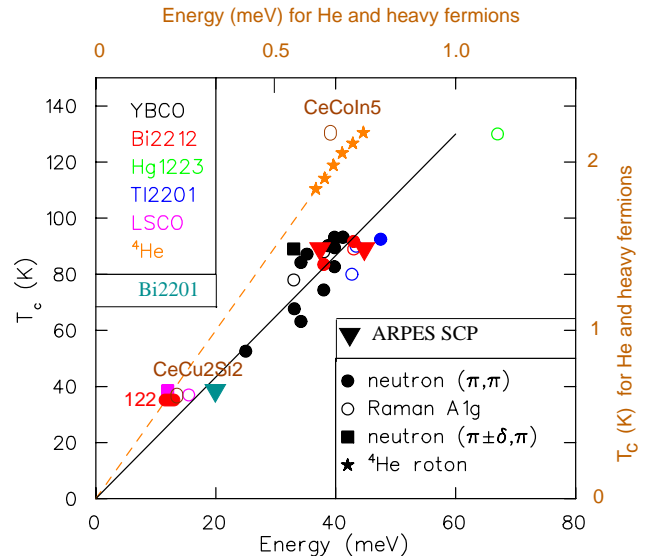


Fig. 3. Plot of T_c versus collective mode energy $\hbar\omega$ for rotons in superfluid ^4He in ambient and applied pressure (orange stars) [45], magnetic resonance mode (MRM) in various cuprates (solid circles) [47], spin-gap energies in LSCO and YBCO (solid squares) [48,49], MRM in $(\text{Ba,K})\text{Fe}_2\text{As}_2$ (red flat solid circle) [50], CeCoIn_5 (brown tall open circle) [51], CeCu_2Si_2 (brown tall open circle) [52], Raman A_{1g} mode energy in cuprates (open circles) [53], ARPES SCP peak energies in cuprates (solid reverse triangles) [54,55]. The horizontal and vertical axes set for He and heavy fermions (brown axis label) has the same aspect ratio as that for other systems (black label), to facilitate comparisons of the slope $T_c/\hbar\omega$.

$\sim 4\text{-}5k_B T_c$ in Fig. 3 can be expected for the roton-like pair-non-breaking excitations as well as for pair-breaking single-particle excitations across the d-wave energy gap. For the former, we shall expect responses sharply localized in momentum space corresponding to the Bragg peak position of the competing magnetic state. In contrast, pair-breaking single-particle excitations must have a broad intensity profile in momentum space. The MRM’s observed in all these exotic superconductors exhibit very sharp profiles in momentum space, supporting our interpretation of collective soft modes associated with competing states. Note that rotons and MRM’s are fluctuations characteristic to first-order quantum phase transitions.

5. Spin-charge twin soft mode and common dispersion relation

As shown in Fig. 3, the energy scale of the MRM spin response is also followed by energies of charge excitations in cuprates, i.e., the A_{1g} response of Raman measurements [53] at the zone center and the superconducting coherence peak (SCP) energy of angle resolved photo emission (ARPES) measurements observed near $(\pi,0)$ [54]. Additionally, Fig. 4e of ref. [55] clearly demonstrates that the ARPES SCP “peak” energy of various cuprate systems corresponds to the neutron MRM energy. Furthermore, the energy-momentum dispersion of the spin and charge soft mode responses are nearly identical to each other, as shown

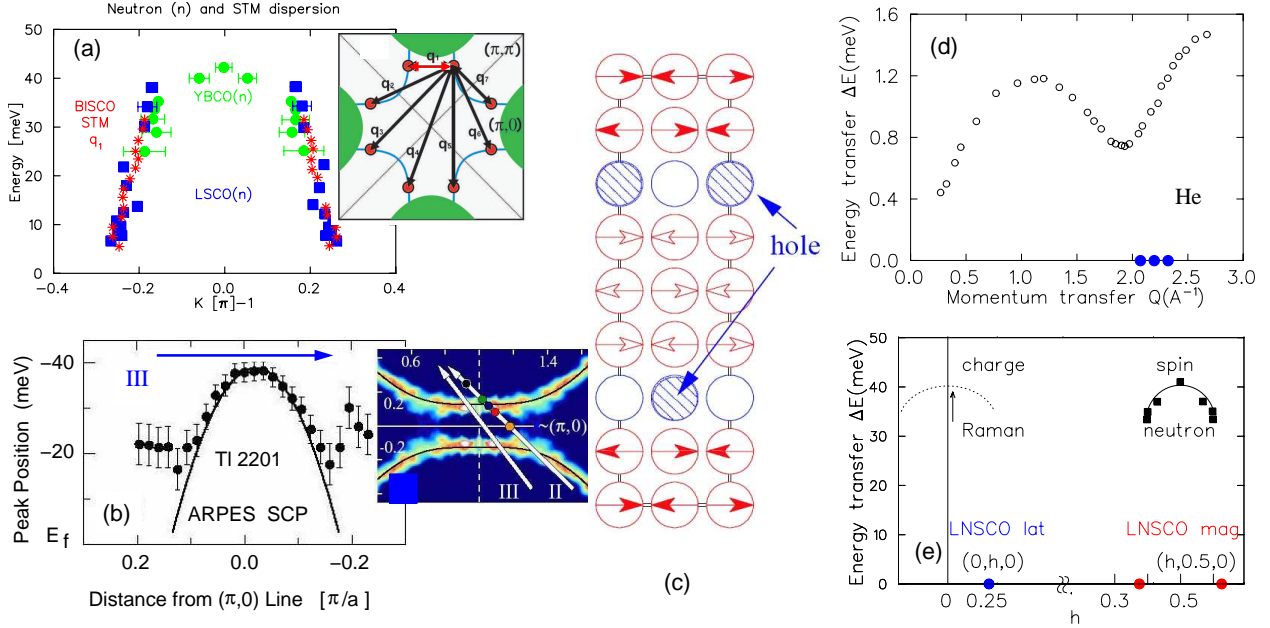


Fig. 4. Dispersion relation of (a) neutron magnetic resonance excitations in YBCO and LSCO [48] cuprates, compared with that of the q_1 charge mode observed in STM [56] in Bi2212, and (b) ARPES SCP peak energy in overdoped Tl2201 near $(\pi,0)$ [57]. (c) Spin-charge correlation pattern for stripe correlations in cuprates [58]. (d) Dispersion relation of rotons in superfluid ^4He [59], with solid circles showing Bragg points of hcp solid He [60]. (e) Proposed dispersion relation for twin spin and charge soft modes in cuprates [6,7] with blue and red solid circles denoting Bragg peaks due, respectively, to charge and spin correlations [58].

by Fig. 4(a) which compares the MRM hour-glass dispersion [48] with that of the low-momentum “ q_1 ” charge mode response in scanning tunneling microscope (STM) measurements [56], and by Fig. 4(b) which shows the energy input for the SCP response of ARPES measurements in the Tl2201 system near $(\pi,0)$ [57].

Figure 4(c) shows the spin-charge modulation pattern of stripe correlations in the cuprates. When the magnetic state wins against the competing superconducting state, this pattern becomes static, accompanied by spin and charge Bragg peaks [58] shown by the solid circles in Fig. 4(e). When the superconducting state wins, this pattern becomes dynamic and short-ranged soft-mode correlations. Even in such a dynamic/inelastic situation, one would expect strong spin and charge coupling. In other words, by paying the energy cost of mode energies, inelastic spin and charge probes detect responses from temporary and short-range stripe patterns. In this situation, it is natural to expect an identical energy cost for the corresponding spin and charge excitations.

The MRM represents collective spin-wave excitations from this short-ranged spin-charge pattern. The excitation energy $\sim 10\text{-}50$ meV of the MRM, much lower than the exchange energy $J \sim 100\text{-}200$ meV in the cuprates, indicates that this process does not involve “pair-breaking” which costs energy J . Similarly, the ARPES SCP peak is produced when a charge is knocked out from the temporary stripe pattern, where no pair-breaking energy J is required thanks to local spin frustration adjacent to charges. Thus, we expect the existence of twin spin and charge excitations, the former near (π, π) and the latter near the zone center, as illustrated in Fig. 4(e) and compared with the

dispersion of rotons in superfluid He [59] and Bragg peaks of hcp solid He [60] in Fig. 4(d). This feature explains why the Raman energy corresponds one-to-one with the neutron MRM energy, instead of the commonly-observed “two-magnon Raman” response appearing with twice the spin excitation energy.

These inelastic collective soft-mode excitations in cuprates are characterized by an unusually strong spin-charge coupling and sharply selective momentum transfers. The strong spin-charge coupling also explains why the excitation of the spin branch in MRM contributes to the depletion of condensed bosons, thus influencing the superconducting T_c analogously to the case of rotons. The closer the superconducting state is to the competing magnetic state, the lower is the energy of the soft-resonance mode, consequently resulting in the lower T_c . Although it is yet to be verified experimentally, one may well expect a similar situation in other strongly-correlated superconductors existing adjacent to competing magnetic states.

6. Spin-charge coupling and pairing via “traffic-light resonance”

Now we shall consider microscopic processes which lead to strong spin-charge coupling, absence of superconductivity in regions with static magnetic order, and strong directional dependence of the charge coherence as found in the difference between nodal and antinodal carriers in the cuprates. Figure 5(a) illustrates charge motion in cuprates in the environment of antiferromagnetic spin correlations. When the spin pattern is static, the hopping motion of a

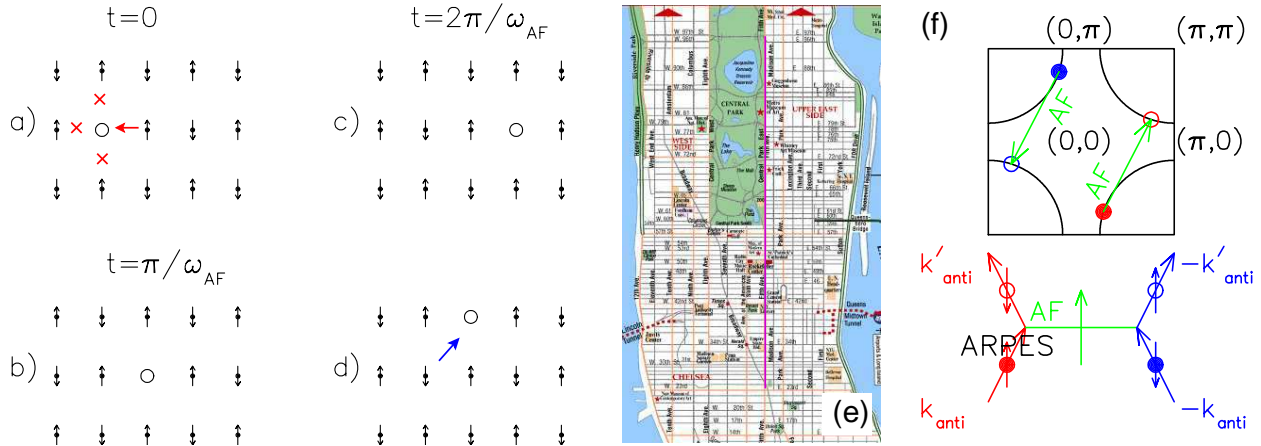


Fig. 5. Illustration of hole motion in cuprates having antiferromagnetic (AF) spin correlations. (a) shows three frustrated bonds created when the AF pattern is static. (b) and (c) depict charge motion occurring sequentially with spin fluctuations. (d) demonstrates no frustration for nodal charges moving diagonally on the same spin sublattice. (e) A map of Manhattan, with Fifth Avenue (purple line) where traffic light alternations are coordinated with the velocity of moving cars. (f) shows pair formation among antinodal charges via scattering of spin fluctuations [6,7].

hole in the antinodal direction (horizontal or vertical direction in Fig. 5(a)) immediately results in an energy cost due to spin frustration. This frustration, however, can be avoided when the hopping occurs sequentially with spin fluctuations. Specifically, when the time scale of the charge motion is comparable to half the period of spin fluctuation (Figs. 5(b) and (c)), a hole can move without the energy cost of spin frustration. This motion can occur successively and coherently, as a resonant charge motion, if, and only if, the charge energy ϵ_F is comparable to that of spin fluctuations $\hbar\omega_{SF}$. For nodal charges propagating in the diagonal direction, this mechanism is irrelevant, since such holes are moving on the same spin sublattice (see Fig. 5(d)).

The propagation of antinodal charges in this process, assisted by and resonating with spin fluctuations, reminds the author of a car or taxi going through synchronized traffic lights. On several avenues in Manhattan alternation of traffic lights are matched with the velocity of cars. For example, on Fifth Avenue (Fig. 5(e) purple line) or Amsterdam Avenue, a car can travel the entire route without being stopped more than a few times. Here the “red” traffic light corresponds to the energy cost due to spin frustration or spin selection rules. Thus, we shall term this spin-assisted charge motion as “traffic light resonance.”

Analogous to the charge motion in a usual metal which causes lattice deformation via electron-phonon coupling, motion of antinodal charges has to be accompanied by the cooperating spin fluctuations. This spin fluctuation can assist motion of another charge with opposite momentum, resulting in an attractive interaction via scattering process as illustrated in Fig. 5(f). Since the charge energy scale ϵ_F is comparable to the energy of mediating bosons (spin fluctuations) $\hbar\omega_{SF}$, this spin-mediated pairing is not retarded, and one can expect a large attractive interaction. This mechanism, occurring selectively for antinodal carriers, is a good candidate for the origin of pseudo-gap formation. Static magnetic order, as frozen traffic lights, inhibits

charge motion and pairing.

This picture for cuprates, with charges dynamically avoiding spin obstacles in cooperation with spin fluctuations, may be generalized to most other correlated electron systems, such as heavy-fermion systems, where the “correlation” originates from spin frustration and/or spin selection rules. In this picture, the “glue” includes all the antiferromagnetic spin fluctuations, with energies extending from the spin gap energy to J . Carriers near the Fermi surface couple with high-energy antiferromagnetic spin fluctuations as $\epsilon_F \sim J$. All the “paramagnon”-like fluctuations, supported by the short-ranged temporal spin-charge correlations, help superconducting coupling as their glues. Thus, the “competing magnetic states” cooperate with superconducting states, supplying the system with useful inelastic fluctuations. Overdoping with $\epsilon_F > J$, however, no longer helps superconductivity, since excessively high-energy charges cannot find their spin partners.

7. Discussions: reconciling conflicting approaches

For many years, theories for cuprates have been discussed in two different approaches. Starting from the parent Mott insulator and underdoped region, which we might call the “left wing” of the phase diagram, one finds relevance to Mott insulator, strong coupling, pre-formed pairs, pseudo-gap, and BE condensation. In these concepts, T_c is related to the particle density, n_s/m^* , T_{BE} and ϵ_F , since pairs are already formed well above the condensation temperature. Most of the arguments in the present paper belong to this “left-wing” approach. The other (“traditional” or “right wing”) approach starts from the overdoped region, involving the concepts of Fermi liquid, BCS condensation, weak coupling, etc., and treating spin fluctuations as perturbations. In the “right-wing” approach, T_c is related to the energy scales of “glues” and attractive interactions, since T_c

implies the pair-formation temperature.

Perhaps a representative work of this latter approach is the spin-fluctuation theory and FLEX approximation by Moriya and Ueda [40]. Identifying spin fluctuations as the mediating bosons in the “right-wing” approach, they generated the plot shown in Fig. 2(c). This figure should be compared and contrasted with the T_c versus ϵ_F plot of Fig. 2(b) which represents the “left-wing” phenomenology. We notice that the energy scale $k_B T_0 \sim \hbar \omega_{SF}$ is very close to ϵ_F estimated from the superfluid density in cuprates and several other correlated-electron superconductors which have relatively high ratios of T_c/ϵ_F . For pairing mechanisms based on the “traffic light resonance,” one requires ϵ_F to be comparable to $\hbar \omega_{SF} \sim k_B T_0$. Therefore, this mechanism naturally leads to “reconciliation” of the left- and right-wing approaches and provides reasoning for why Figs. 2(b) and 2(c) look alike for some cuprate and heavy fermion systems. On the other hand, it should also be noted that models developed from the “right wing” approach do not explain correlations between T_c and n_s/m^* in the underdoped region shown in Fig. 2(a).

Another apparent duality can be found in the role of competing magnetic states on superconductivity. The soft-mode argument identifies closeness to the magnetic state as a destructive factor which reduces the superconducting T_c . The “traffic light resonance,” however, requires an inelastic excitation associated with dynamical correlations originating from the competing magnetic state. Charge doping will help increase T_c as shown in Figs. 2(a) and (b), while excessive charge doping would destroy/weaken the magnetic correlations required for pairing. This duality should be the origin of formation of the superconducting dome in phase diagrams of cuprates and several other systems.

One remaining challenge for our phenomenology is to understand the origin of an apparent upper limit $T_c/T_{BE} \sim 1/4$ suggested by Fig. 2(b). Better understanding of the interplays between spins and charges, the left- and right-wing approaches, superconducting and magnetic states, and BE-BCS crossover would hopefully explain this trend.

8. Acknowledgments

The author would like to thank collaborations with G.M. Luke, T. Goko, E. Saitovitch, H. Kageyama and many other scientists coauthoring refs. [14-16,19,22,25,28,29,31,34,37-39,41,42] in experiments on various exotic superconductors and magnets, and H. Aoki and K. Ueda for discussions on the Moriya-Ueda theory. This work is supported by the NSF MWN-CIAM program DMR 05-02706, 08-06846.

References

[1] Y. Kamihara *et al.*, J. Am. Chem. Soc. **130** (2008) 3296.

[2] X.H. Chen *et al.*, Nature **453** (2008) 761; G.F. Chen *et al.*, Phys. Rev. Lett. **100** (2008) 247002; Zhi-An Ren *et al.*, Europhys. Lett. **83** (2008) 17002.
 [3] M. Rotter *et al.*, arXiv:0805.4630; G.F. Chen *et al.*, arXiv:0806.1209 (2008).
 [4] M.S. Torikachvili, S.L. Bud’ko, Ni Ni, P.C. Canfield, Phys. Rev. Lett. **101** (2008) 057006.
 [5] P.L. Alireza *et al.*, arXiv:0807.1896 (2008).
 [6] Y.J. Uemura, J. Phys. Condens. Matter **16**, S4515-S4540 (2004).
 [7] Y.J. Uemura, Physica **B374-375**, 1-8 (2006).
 [8] C. de la Cruz *et al.*, Nature **453** (2008) 899.
 [9] Q. Huang *et al.*, arXiv:0806.2776 (2008).
 [10] A.I. Goldman *et al.*, arXiv:0807.1525 (2008).
 [11] H.H. Klauss *et al.*, arXiv:0805.0264 (2008).
 [12] H. Luetkens *et al.*, arXiv:0804.3115 (2008); R. Khasanov *et al.*, arXiv:0805.1923 (2008).
 [13] A.J. Drew *et al.*, arXiv:0805.1042 (2008).
 [14] J.P. Carlo *et al.*, arXiv:0805.2186 (2008).
 [15] A.A. Aczel *et al.*, arXiv:0807.1044 (2008).
 [16] T. Goko *et al.*, arXiv:0808.1425 (2008).
 [17] M. Rotter *et al.*, arXiv:0805.4021 (2008).
 [18] A. Jesche *et al.*, arXiv:0807.0632 (2008).
 [19] T. Goko *et al.*, unpublished results.
 [20] H. Luetkens *et al.*, arXiv:0806.3533 (2008).
 [21] A.J. Drew *et al.*, arXiv:0807.4876 (2008).
 [22] J. Zhao *et al.*, arXiv:0806.2528 (2008).
 [23] H. Lee *et al.*, arXiv:0809.3550 (2008).
 [24] A.T. Savici *et al.*, Phys. Rev. **B66**, 014524 (2002).
 [25] K.M. Kojima *et al.*, Physica **B 326**, 316-320 (2003).
 [26] H.E. Mohottala *et al.*, Nature Materials **5**, 377-382 (2006).
 [27] T. Sasaki, N. Yoneyama, N. Kobayashi, Phys. Rev. **B77** (2008) 054505
 [28] J. Arvanitidis, J. Phys.: Condens. Matter **19** (2007) 386235.
 [29] Luke, G. M. *et al.*, Phys. Rev. Lett. **73**, 1853-1856 (1994).
 [30] G. Knebel, D. Aoki, J.P. Brison, J. Flouquet, arXiv:0808.3687, J. Phys. Soc. Japan (2008) in press.
 [31] Y.J. Uemura *et al.*, arXiv:0806.2021 (2008).
 [32] T. Yildirim, arXiv:0804.2252 (2008).
 [33] Q. Si, E. Abrahams, arXiv:0804.2480 (2008).
 [34] Y.J. Uemura *et al.*, Phys. Rev. Lett. **62** (1989) 2317.
 [35] J.E. Sonier, J.H. Brewer, R.F. Kiefl, Rev. Mod. Phys. **72** (2002) 769.
 [36] *Muon Science: Muons in Physics, Chemistry and Materials*, ed. by S.L. Lee, S.H. Kilcoyne, and R. Cywinski, Inst. of Physics Publishing, Bristol, 1999.
 [37] Y.J. Uemura *et al.*, Phys. Rev. Lett. **66** (1991) 2665.
 [38] Y.J. Uemura *et al.*, Nature **352** (1991) 605.
 [39] L.P. Le *et al.*, Phys. Rev. Lett. **68** (1992) 1923.
 [40] T. Moriya and K. Ueda, Rep. Prog. Phys. **66** (2003) 1299; Adv. Phys. **49** (2000) 555; and references therein.
 [41] C. Stassis *et al.*, Phys. Rev. **B33** (1986) 1680.
 [42] Y.J. Uemura *et al.*, Phys. Rev. **B33** (1986) 6508.
 [43] J. Zhao *et al.*, arXiv:0808.2455 (2008).
 [44] J. Ruvalds, Phys. Rev. Lett. **27** (1971) 1769.
 [45] O.W. Dietrich, E.H. Graf, C.H. Huang, L. Passell, Phys. Rev. **A5** (1972) 1377.
 [46] J.M. Kosterlitz and D.J. Thouless, J. Phys. **C: Solid State Phys.** **6**, (1973) 1181.
 [47] P. Bourges *et al.*, Physica **C424** (2005) 45.
 [48] N.B. Christensen *et al.*, Phys. Rev. Lett. **93** (2004) 147002.
 [49] J.M. Tranquada *et al.*, Nature **429** (2004) 534.
 [50] A.D. Christianson *et al.*, arXiv:0807.3932.
 [51] C. Stock, C. Broholm, J. Hudis, H.J. Kang, and C. Petrovic, Phys. Rev. Lett. **100** (2008) 087001.
 [52] O. Stockert, *et al.*, Physica **B403** (2008) 973.
 [53] Y. Gallais *et al.*, Phys. Rev. Lett. **88** (2002) 177401.
 [54] A. Damascelli, Z. Hussain, Z.X. Shen, Rev. Mod. Phys. **75** (2003) 473 (see Fig. 50 at p. 513).

- [55] J. Wei *et al.*, Phys. Rev. Lett. **101** (2008) 097005.
- [56] K. McElroy *et al.*, Nature **422** (2003) 592.
- [57] M. Platié *et al.*, Phys. Rev. Lett. **95** (2005) 077001.
- [58] J.M. Tranquada *et al.*, Nature **375** (1995) 561.
- [59] D.G. Henshaw and A.D.B. Woods, Phys. Rev. **121** (1961) 1266.
- [60] D.G. Henshaw, Phys. Rev. **109** (1958) 328.